

Demonstration of an improved passive acoustic fault detection method on recordings from the Phénix steam generator operating at full power

Anders Riber Marklund, Frédéric Michel, Henryk Anglart

▶ **To cite this version:**

Anders Riber Marklund, Frédéric Michel, Henryk Anglart. Demonstration of an improved passive acoustic fault detection method on recordings from the Phénix steam generator operating at full power. Annals of Nuclear Energy, 2017, 101, pp.1-14. 10.1016/j.anucene.2016.10.003 . cea-02388892

HAL Id: cea-02388892

https://cea.hal.science/cea-02388892

Submitted on 2 Dec 2019

HAL is a multi-disciplinary open access archive for the deposit and dissemination of scientific research documents, whether they are published or not. The documents may come from teaching and research institutions in France or abroad, or from public or private research centers.

L'archive ouverte pluridisciplinaire **HAL**, est destinée au dépôt et à la diffusion de documents scientifiques de niveau recherche, publiés ou non, émanant des établissements d'enseignement et de recherche français ou étrangers, des laboratoires publics ou privés.

Demonstration of an improved passive acoustic leak detection method on recordings from the Phénix steam generator operating at full power

Anders Riber Marklund[a,*], Frédéric Michel[b], Henryk Anglart[a]

[a] *KTH Royal Institute of Technology, Division of Nuclear Reactor Technology AlbaNova University Center, 10691 Stockholm, Sweden*
[b] *CEA CAD/DEN/DTN/STCP/LIET, Bâtiment 202, 13108 Saint-Paul-lez-Durance, France*

Abstract

A hidden Markov model method proposed earlier for passive acoustic leak detection in sodium fast reactor systems has been improved to eliminate ad-hoc setting of model parameters and allow smaller amounts of training data. The method is based on training the hidden Markov model on known background noise only and optimizing its free model parameters by a parametric study of detection performance for synthetic noises superposed onto the same background noise. Using recordings of background noise as well as from argon injection tests performed at full power in the Phenix sodium fast reactor plant, it is estimated that the resulting method will detect leak-like deviations from the background noise with a detection delay of 3 seconds, a false alarm rate close to 10^{-8} and at signal-to-noise ratio conditions at least corresponding to an additive signal at -10 dB. The method is one-channel, i.e. using input from one single acoustic sensor only.

Keywords: Sodium fast reactors, Acoustic leak detection, Fault detection algorithms, Hidden Markov models

1. Introduction

Sodium fast reactors (SFRs) are fast reactor designs using liquid sodium as coolant. As, almost without exception, all nuclear power plants use steam turbines to drive the generator set, existing SFRs use or have used sodium heated steam generators to transfer energy from the secondary to the tertiary circuit [1]. Sodium heated steam generators however present an inherent risk in the case of a leak between its two circuits. As sodium and water have a quite

*Corresponding author.
Email addresses: andersrg@kth.se (Anders Riber Marklund), michel.frederic@cea.fr (Frédéric Michel), henryk@kth.se (Henryk Anglart)

violent chemical reaction, releasing additional heat and corrosive reaction products, such a leak can damage other steam generator tubes nearby and create a self-accelerating damage process [2]. The task of detecting leaks has therefore always been important for SFR steam generator monitoring equipment, generally achieved through the use of chemical hydrogen detection systems with relatively slow response [3]. Acoustic leak detection systems have been an interesting alternative for a long time due to their much shorter response times and relative simplicity but have never reached further than the experimental stage. Some overviews of work on the topic can be found in [2] and [4].

Within the ASTRID project [5], the Commisariat a l'Énergie Atomique et aux Énergies alternatives (CEA) is currently studying the option of using a Brayton cycle energy conversion system for SFRs with nitrogen as tertiary fluid. The steam generators would in this design be replaced by compact sodium-nitrogen heat exchangers. Even if the risk of violent chemical reaction is thereby excluded, hydrodynamic effects affecting both safety and performance of the heat exchanger, as well as the risk of a gas leak over to the primary system still motivate using a leak detection system as part of the continuous monitoring equipment.

The noises of small leaks will be due to aeroacoustic jet noise, fluid-structure interaction, sodium-water reaction (for the steam generator case) and the acoustic effects of bubble populations (absorption, scattering, diffusion and resonance) [6], [7]. The relative importance of these effects will depend on the leak rate, leak geometry, ambient conditions as well as the acoustic wave propagation path from the leak position to the acoustic sensor. Furthermore, neither measurement nor experimental simulation of realistic leak signals in a nuclear power plant are assumed to be possible. These facts taken together motivates aiming for a method that learns to recognize normal operation background noise and detects any deviation from this known noise.

In this work we develop such a method, based on a hidden Markov model concept proposed in [8]. The performance is assessed by applying it to recordings from argon injection tests performed in the Phenix steam generator at full power. Section 2 contains a description of these tests and the recording data. Section 3 describes the improved hidden Markov model detector method and how detector performance is measured. The results, presented in section 4, starts with a short discussion of what is actually detected in the Phenix recordings. Then, a study of detector parametrizations is made, and the results of this study in detection of synthetic testing signals superposed on the background noise are used to choose a detector parametrization. A final demonstration is then made on the argon injection data as well as on pure background noise. Detection delay, false alarm rate and detectable additive SNR for the proposed method are all estimated.

Discussion of the method and our results as well as conclusions and some ideas for future work are given in section 5 and 6.

Table 1: Studied recordings

Recording no.	Recording length [s]	Injection length [s]	P_{Ar} [bar]	f_s [Hz]
1	600.0	0.0	-	25600
2	300.0	20.0	7	51200
3	300.0	20.0	6	51200
4	300.0	20.0	5	51200
5	116.6	60.0	8	51200
6	300.0	60.0	8	51200

2. Experimental data

2.1. Argon injection tests at the Phenix SFR

In 2008 and 2009, a series of tests were carried out in the Phenix SFR plant with the aim of studying feasability of a passive acoustic leak detection system for the steam generators. During these tests, leaks were simulated by performing argon injections in a sodium inlet line to the steam generator. Five acoustic sensors of type ENDEVCO 7704 A were placed on sodium lines connected to the steam generator according to figure 1.

During a first acoustic measurement campaign in late 2008, 600 s of normal full-power background noise was recorded with a sampling rate of 25600 samples/s. Later, in May 2009, the actual recordings of argon injection tests were made, for some reason at a doubled sampling rate. Several injections of various durations and driving pressures were performed. In each test, the injection was started about 35 s after the recording start, injection durations ranged from 5 to 60 s and the recording length was 300 s in most cases. Six of the resulting recordings (including the pure background noise) have been made available by the CEA for use in this article. Characteristics of the analyzed recordings are shown in table 1 and the raw signals are shown in figure 2. Figure 3 shows the corresponding time-frequency evolution up to the lower Nyquist frequency of 12.8 kHz. For the signal on sensor 1, located closest to the injection point, figure 4 shows power spectral density estimates of the signal for background noise as well as for the 5 argon injection tests. The two 8 bar injections can be distinguished towards the end of the sensor 1 signal in figure 2. The other three injections are barely noticeable. Some impulsive behaviour is visible on the signals of sensors 2-4 and at the end of the sensor 5 signal. From figures 3 and 4 it is clear that the injections lead both to acoustic emission and absorption. The injection effects seen in figure 3 also seem to be somewhat delayed for each sensor, indicating that bubbles from the injection are detected as they are transported by the circulating sodium. This effect was also noted in an internal CEA document [9] and will be verified in some more detail in sections 4.1 and 4.4.

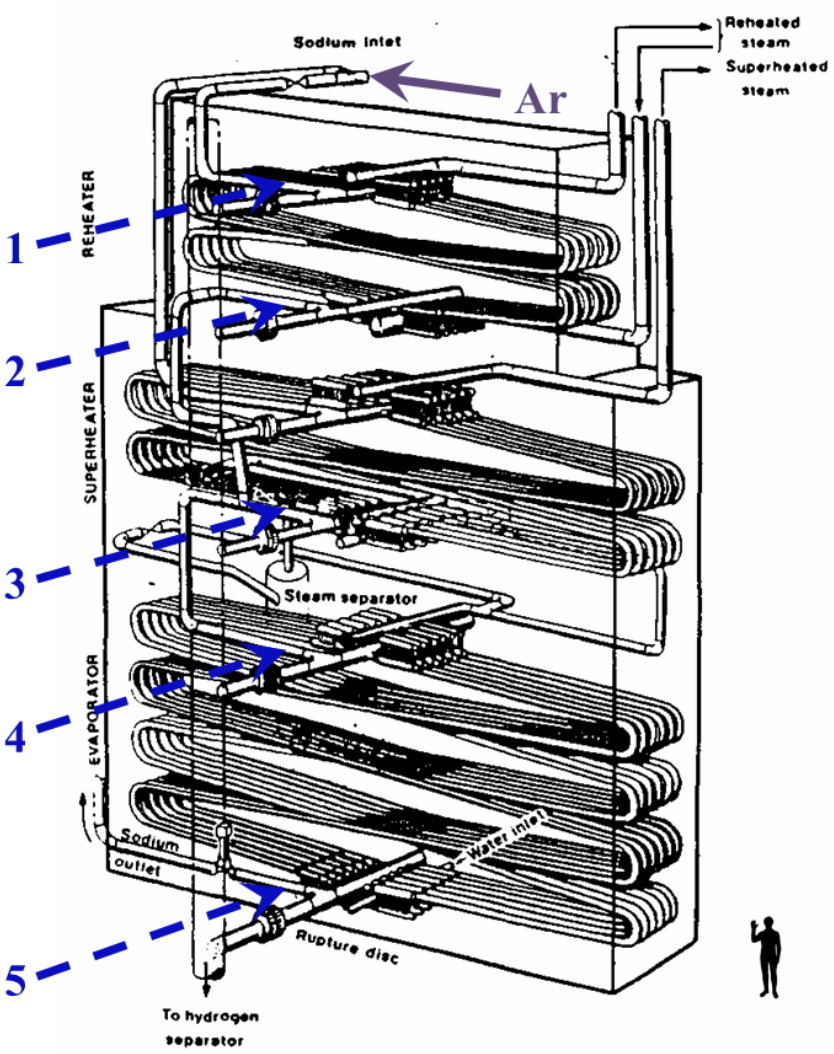


Figure 1: Schematic view of the Phenix steam generator indicating approximate positions of the five acoustic sensors and argon injection system used in the 2008-2009 tests.

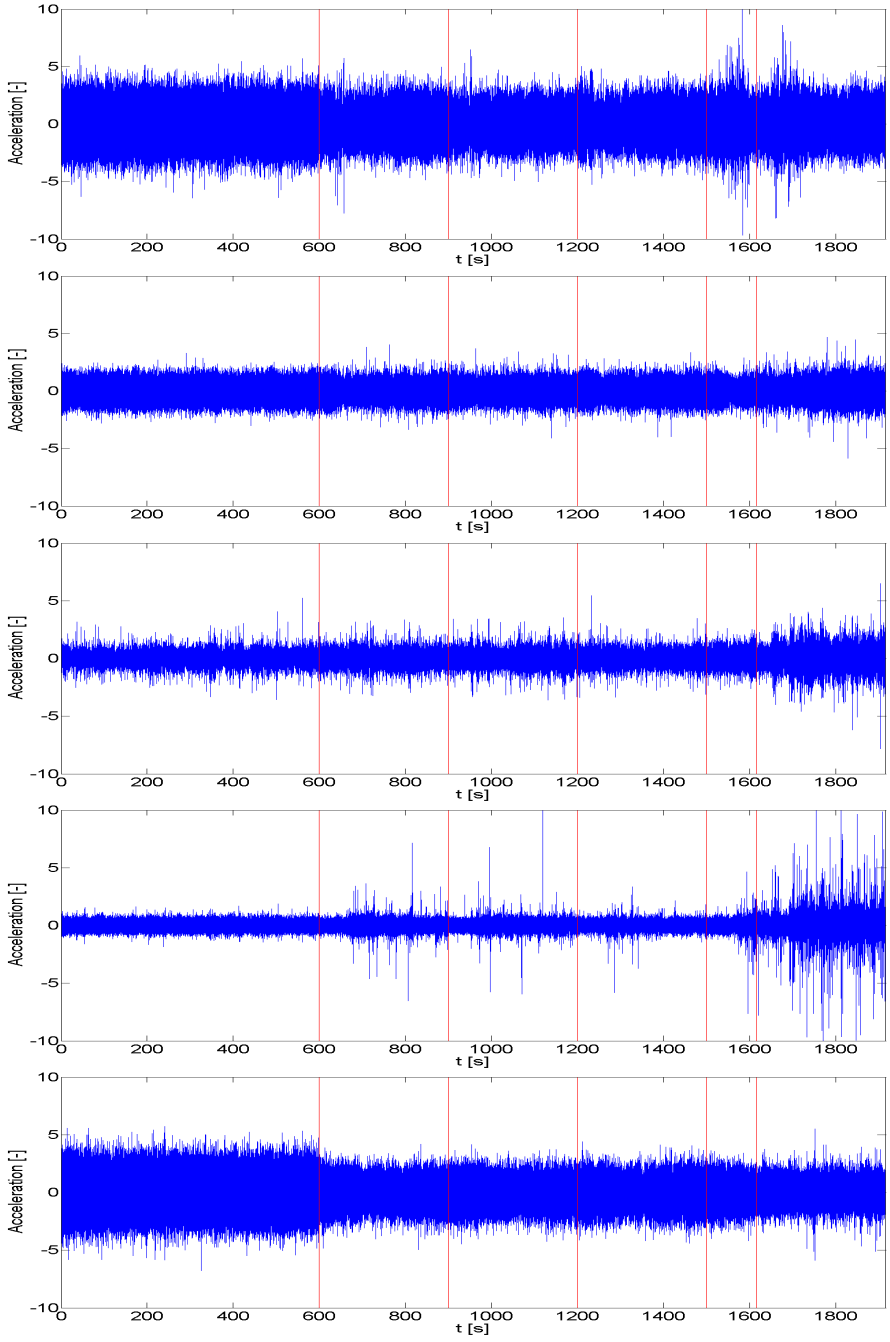


Figure 2: Raw acoustic signals (acceleration) of all studied recordings with recording breaks indicated by vertical lines and responses of sensors 1 to 5 displayed from top to bottom.

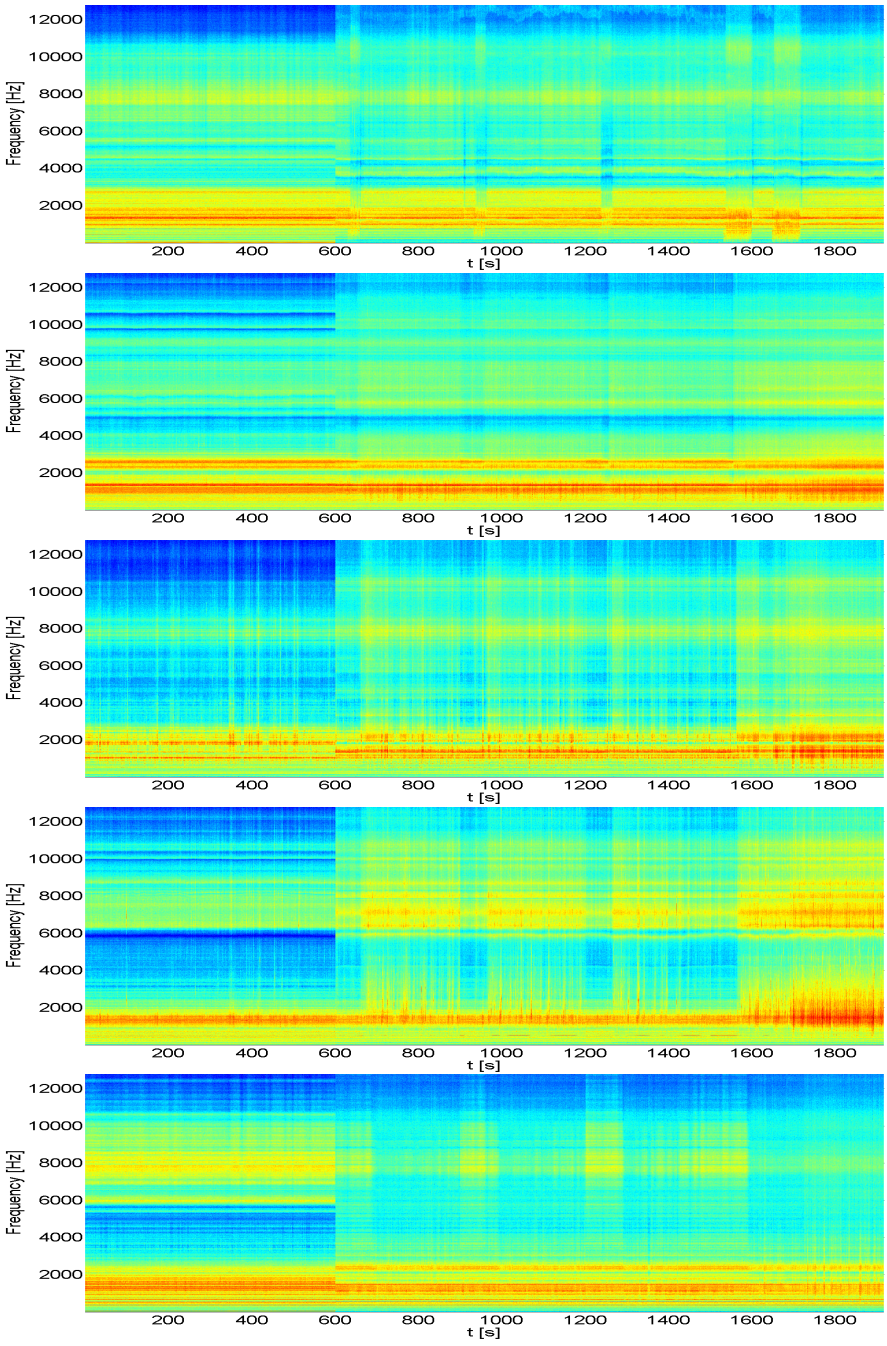


Figure 3: Time-frequency evolution of all studied recordings on sensors 1 to 5, displayed from top to bottom. (The common sampling rate and thereby the Nyquist frequency of all recordings is limited by recording 1.)

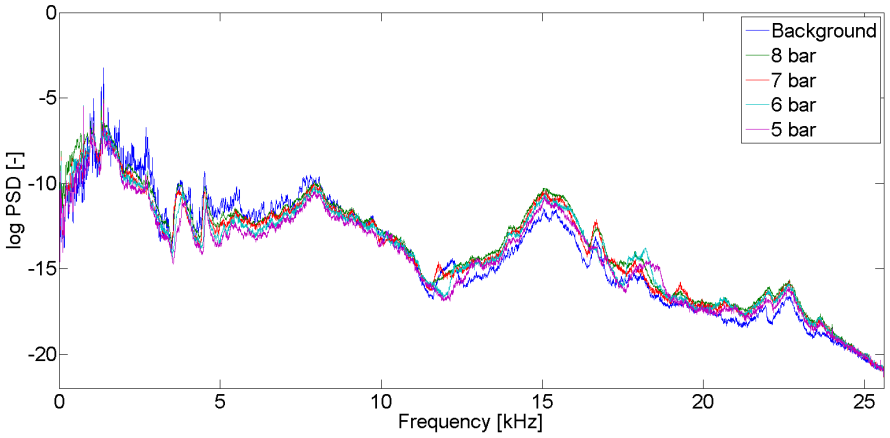


Figure 4: Power spectral density estimates of the recorded signal at sensor 1.

3. Detection method

3.1. Improved HMM detector

Hidden Markov models (HMMs) with Gaussian mixture models (GMMs) as emission probabilitites have been widely used in various speech recognition applications [10]. The actual data modeled for human speech is often so-called mel frequency cepstrum coefficients, extracted from the measured audio signal in a way that imitates the functioning of the human ear [11]. For our application, i.e. fault detection in industrial acoustic noise signals, a new feature calculation scheme based on the Welch PSD estimate [12] was presented in [8] along with some basic HMM theory. A brief review of this scheme explicitly stating the improvements that are new to this work will now be given.

We denote the PSD estimate of the time discrete signal $x(t_n)$ with $X(f_j)$, where t_n are the signal sampling times and f_j are the frequency bands. The average PSD of a normal operation signal is denoted X_0. We monitor the residual XR from this model over sliding time windows of constant length tw, enumerated by m and we propose a componentwise normalization of the residual, i.e.

$$XR(f_j, m) = \frac{X(f_j, m) - X_0(f_j)}{X_0(f_j)} \tag{1}$$

Contrary to the normalization used in [8], this residual will not be indifferent to pure multiplicative changes in the signal, but it can be assumed that such changes can be identified by a parallell algorithm if needed.

In each time window, a vector of PSD component indices ordered by current residual size is also created, i.e.

$$J_k(m) = \left\{ j_k | XR(f_{j_k}, m) > XR(f_{j_{k+1}}, m) \right\} \tag{2}$$

where the integer k enumerates its components. Based on $XR(f_j, m)$ and $J_k(m)$ we now introduce a modified feature calculation scheme compared to the one of [8], given by

$$\mathbf{F}(m) = F_k(m) = J_k(m) + \beta \log \sum_j |XR(f_j, m)| \quad , \quad k = 1, ..., k_{max} \tag{3}$$

The second term on the right represents the log of the total power deviation over all studied frequencies while the first term, for each k, points out the frequency band at which the PSD estimate is currently deviating the most, secondmost, thirdmost et c from its average value on the training data. The first term takes on discrete values from 1 to j_{max}. The second term, which takes on real number values, is rescaled to cover approximately the same domain by calculating the factor β according to

$$\beta = \frac{j_{max}}{2\sigma_{XR}} \tag{4}$$

where

$$\sigma_{XR}^2 = E\left[(d_{XR}(m) - \mu_{d_{XR}})^2\right] \tag{5}$$

and

$$d_{XR}(m) = \log \sum_j |XR(f_j, m)| \tag{6}$$

i.e. σ_{XR} represents the estimated standard deviation of the second term of equation 3 over the training data.

The relative importance factor of the first and second term of the feature, β, was in our previous work set by an ad-hoc trial and error procedure [8]. Since we are aiming for a method to be licensed for safety related systems in nuclear power plants, basing the method on well-defined and predictable procedures is of utmost importance. The introduction of equation 4 in this respect represents an important improvement of the scheme. Furthermore, the new normalization of equation 1 has been introduced in order to allow considerably smaller amounts of data in the training sequence while maintaining detector performance. In [8], training periods of about one minute were needed for a signal sampled at 200 kS/s. Using the scheme presented here, training periods of 20 s are sufficient, even on the signals with a sampling frequency of 25600 S/s, i.e. reduction by a factor of 24 of the amount of training data needed.

We now remind the reader that the model parameters of an HMM are set by applying a so-called *training algorithm* to an observed feature sequence $\mathbf{F}(m)$. The training is done by local likelihood maximization using the Baum-Welch algorithm [10]. When presented with a new feature sequence, it is then possible to calculate a conditional probability that the observed sequence is generated by the trained model by a recursive algorithm. In practice, the logarithm of this conditional probability is used in order to avoid computation problems due to small numbers [11]. I.e. after training a model λ_{bg} on acoustic normal operation background noise, the following expression is used as a discriminant for fault detection

$$d_{HMM}(m) = \log(P(\mathbf{F}(m)|\lambda_{bg})) \tag{7}$$

In [8], the *model quality* was studied as a function of the HMM model parameters only by reapplying the trained models to testing data on the same signal type. Here we will instead study the actual *detection performance* as a function of both the free model, and the free feature scheme parameters. The full set of studied parameters then becomes:

- The sliding window length tw
- The size of the feature vector, k_{max}
- The number of Gaussians in the GMM, G
- The number of states in the HMM, S

3.2. Detector performance measures

A standard way of assessing the performance of a discriminant for detection is to calculate a *receiver operating characteristic*, or ROC, curve [14]. A common scalar measure of the detection performance is the area under the ROC curve. For detectors that have maximal area under the ROC curve, this measure can not be used to distinguish their performance. We therefore also use a min-max margin measure, similar to the one used in [13]. For discriminants d that are designed to decrease at the onset of detection, this measure is defined by

$$mmd = \frac{\min d_1}{\max d_0} \tag{8}$$

where d_1 and d_0 are the discriminant outputs in a known detection region and a known normal background region, respectively.

4. Results

For recordings 2-6, the training period used for each sensor channel extended from 5 to 20 seconds into the signal, for reasons that will be clear later. For recording 1, a training period from 120 to 220 seconds was used. The average background PSD estimate X_0 and the feature sequence $\mathbf{F}(m)$ used for training of HMMs was thus calculated on these periods.

4.1. Physical interpretation

It is instructive to study the nature of the acoustic signals by some basic change measure before going on to testing of the more sensitive HMM method. By listening to the actual recording from sensor 1 it was found that a tone-like sound appears a few seconds before the response in the higher frequencies. The proposed interpretation of this fact is that the injection itself creates a fairly weak low-frequency whistle and then the argon bubbles, a little later, create a high-frequency "trickle" noise as well as acoustic absorption as they reach the acoustic sensor position.

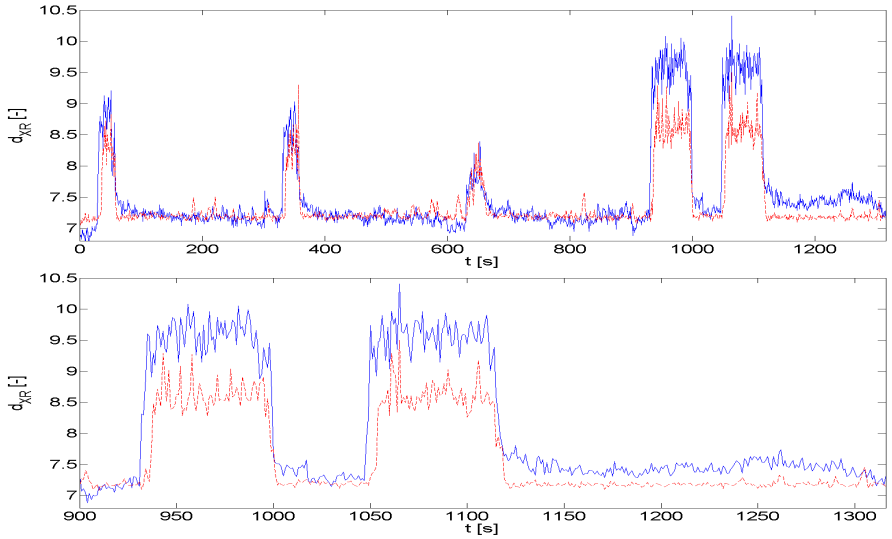


Figure 5: Upper panel: Low (solid line) and high (dashed line) frequency discriminants applied to sensor 1, recordings 2-6. Lower panel: Zoom on recordings 5 and 6.

As a simple demonstration, the discriminant defined by equation 6 was calculated for low (0 - 2 kHz) and high (21 - 26.5 kHz) frequencies on recordings 2-6 from sensor 1. The resulting log power deviations are shown in figure 5. We found that the response of the low-frequency discriminant appears 5-7 seconds before the high-frequency discriminant.

Next, the high-frequency deviation discriminants of recording 2 are shown for all sensors in figure 6. Here, it can be seen that the response is somewhat delayed for each sensor, and extended for sensors 2-5, corresponding to a hypothesis of argon bubbles traveling trough the steam generator and spreading out. The delays are larger from sensor 1 to 2 as well as from sensor 4 to 5. This corresponds well to the positioning of the sensors and the piping configuration (c.f. figure 1) where the bubbles pass through the longer S-shaped tubes only between sensors 1 and 2 and sensors 4 and 5. From sensor 2, at the reheater sodium outlet, to sensor 4 at the evaporator inlet, the bubbles travel through shorter piping, bypassing the superheater S-tubes.

The secondary sodium inventory of the Phenix plant was about 140000 kg per loop and the secondary sodium flowrate was about 800 kg/s. From these values, a sodium circulation period time for the secondary circuit of about 175 s is found. It is however reasonable to assume that some of the secondary sodium remained stationary in a storage tank and did not circulate, thus leading to a shorter period time. The fluctuations seen in the response of the first sensor about 150 s after injection start in figure 6 can therefore probably be attributed to argon bubbles returning after completing one lap in the secondary circuit.

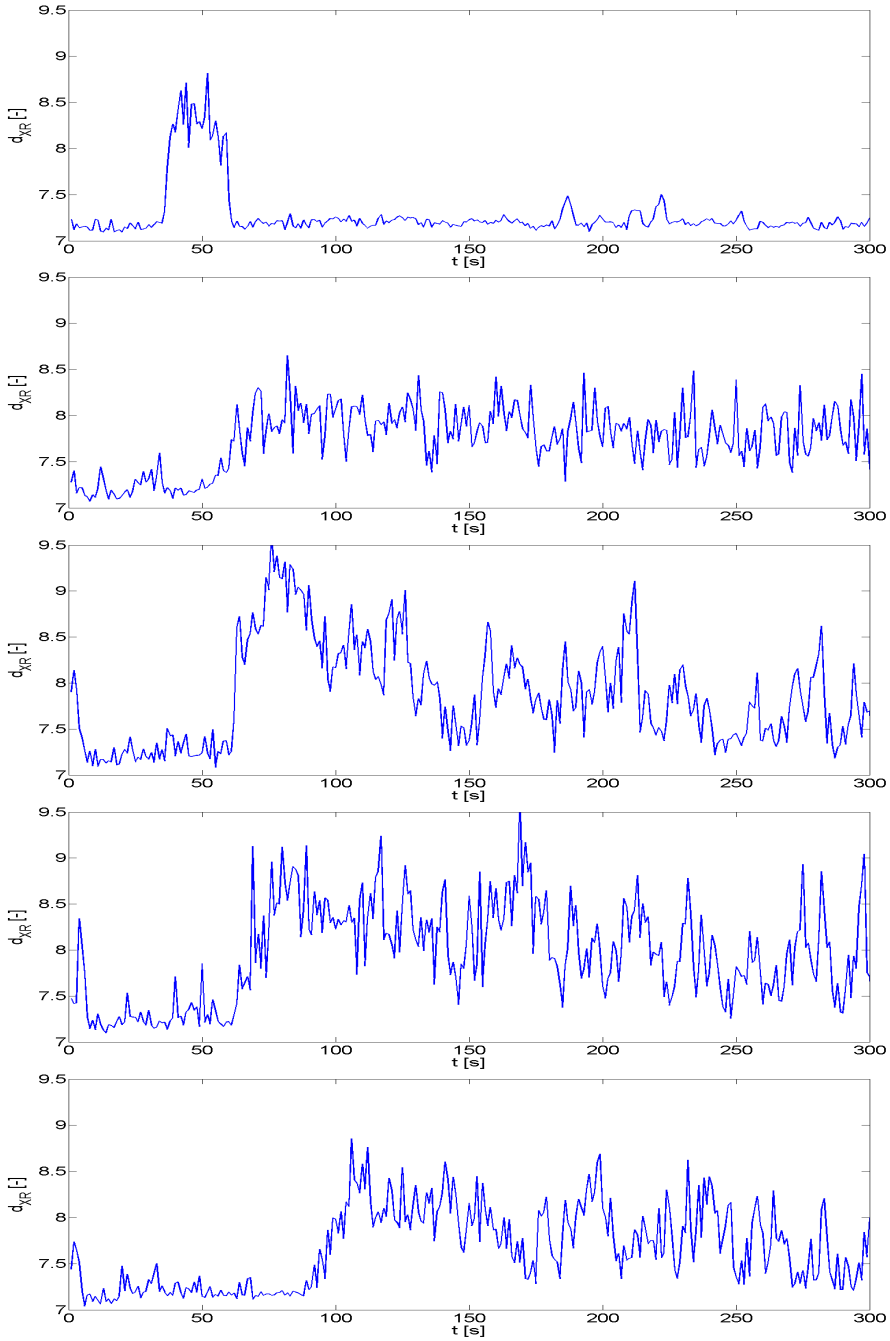


Figure 6: High frequency energy deviation discriminant applied to sensors 1-5, recording 2.

Table 2: Studied parameters

Parameter	Range	Unit
tw	800, 1024, 1280, 1600, 2560, 3200	[samples]
S	1,2,3,4	[-]
k_{max}	1,2,3,4	[-]
G	1,2,3,4	[-]

4.2. Parameter study on synthetic test signals

The parameters studied are listed in table 2. The values for the sliding window length are defined by numbers yielding an integer number of windows on one second of data (at the lower sampling rate of 25.6 kHz). The cases having $S = 1$ represent pure GMMs, i.e. they lack time evolution modeling and are technically not hidden Markov models.

If the best detector would have to be found by a parametric study on injection noise data similar to recordings 2-6, the method would not be independent of such data. Instead, an approach where synthetic testing signals are superposed onto the normal background noise will be used here, i.e.

$$x(t_1, ..., t_2) = x_{bg}(t_1, ..., t_2) + Cx_{test} \tag{9}$$

where C is a constant factor and the testing sigal duration $t_2 - t_1$ was chosen to be 100 seconds. The first testing signal was a white Gaussian noise and the second one was a stationary signal with stochastic phase, created from a PSD of the background noise, using the same method as in [13]. The latter case is in some respect limiting, as it corresponds to detection of a stationary noise which has maximal resemblance to the background. For signals superposed in this way, an advantage is that the resulting signal-to-noise ratio can be controlled by the factor C and straightforwardly calculated from the definition

$$SNR = 10 \log_{10} \frac{P_{test}}{P_{bg}} \tag{10}$$

where P_{test} and P_{bg} are the signal powers of Cx_{test} and x_{bg} respectively. A measure of the signal power is obtained by summing the PSD components up to the Nyquist frequency.

Putting ourselves in the position of having to parametrize the detector without acces to injection test data we now demonstrate how this can be done using only the synthetic testing signals and a simplistic parameter study. During this study, the background-like noise was added at $SNR = -2$ dB and the white Gaussian noise at $SNR = -28$ dB. The min-max distance is shown as function of time window length in figure 7. A local maximum is present at 2560 samples. Now restricting ourselves to parametrizations with $tw = 2560$ and $S > 1$, the min-max distance is shown as function of k_{max} in figure 8. The performance

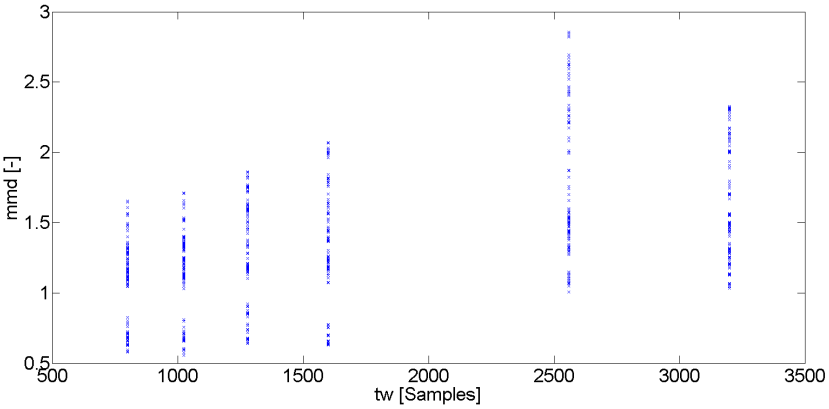


Figure 7: Min-max distance of synthetic testing signals versus tw.

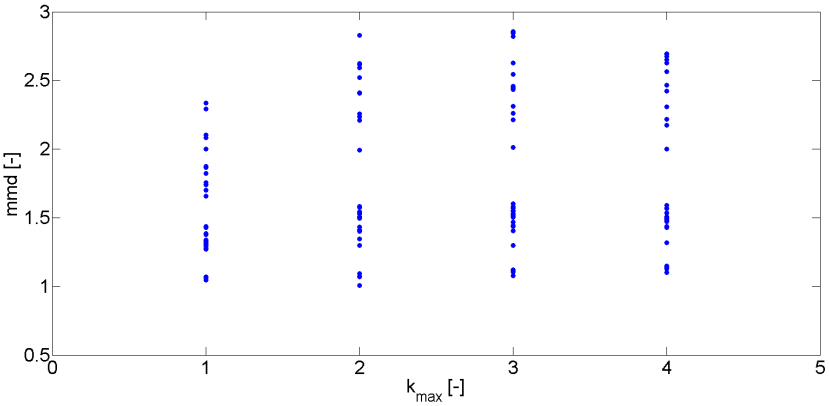


Figure 8: Min-max distance of synthetic testing signals versus of k_{max} for $tw = 2560$.

can be seen to be split into two groups, corresponding to the two testing signals. For k_{max} values larger than 1 there is no clear trend, but the performance seems to deteriorate at $k_{max} = 4$, so we choose $k_{max} = 2$ to promote smaller models. Finally, the performance as function of G and S is shown in figure 9. Larger models are seen to give slightly higher min-max distance. In a future application, more testing signals could be studied and a more sophisticated approach based on the response surface could be used to pick the parametrization with optimal performance. As the amount of training data was in some cases slightly too small for the larger values of G and the spread in performance seem to increase at $S = 4$, we here chose $tw = 2560$, $k_{max} = 2$ $G = 3$ and $S = 3$ as the final parametrization. Since $tw = 2560$ yields 10 sliding windows per second at 25600 samples per second, we will denote this model by HMM10233.

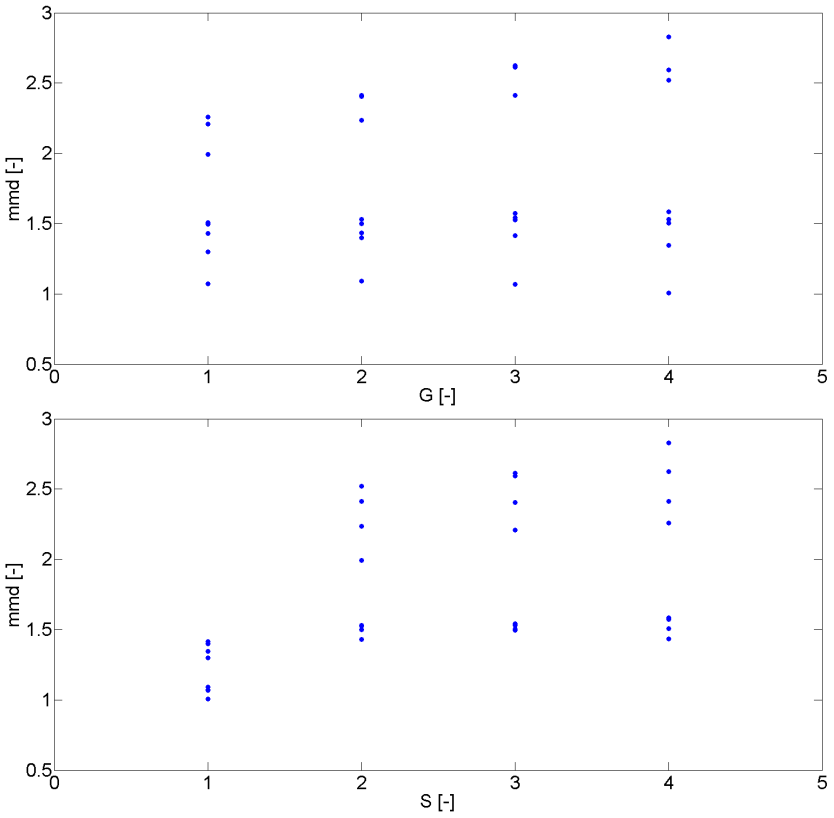


Figure 9: Min-max distance of synthetic testing signals versus G and S for $tw = 2560$ and $k_{max} = 2$.

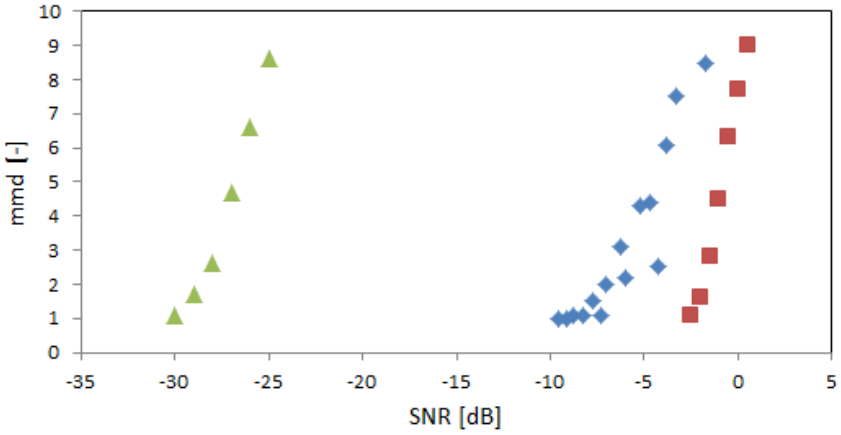


Figure 10: Min-max distance as function of additive SNR for WGN (triangles), 8 bar argon injection (diamonds) and background-like noise (squares).

4.3. Detectable SNR studies

In another study, the detectable SNR for the HMM10233 was studied, defining "detectable" as cases having a min-max distance larger than 1, i.e maximal area under the ROC. When analyzing the synthetic testing signals, the detectable signal power was found by gradually decreasing the superposition factor C of equation 9 and thereby also the SNR as calculated by equation 10. For the 8 bar argon injection signals, a changed SNR was first estimated on the raw signal according to

$$SNR_\Delta = 10 \log_{10} \frac{P_\Delta}{P_0} \tag{11}$$

where

$$P_\Delta = \sum |X_1 - X_0| \quad \text{and} \quad P_0 = \sum X_0 \tag{12}$$

where X_0 and X_1 are the average PSD estimates in the background and the injection region of the signal respectively. By this method it was found that $SNR_\Delta \approx -1.1$ dB for the 8 bar injections. The detection performance at lower SNRs was then investigated by superposing additional stationary background noise onto the injection signal, as was done also in a study on injection test recordings from the PFR [13]. The resulting min-max distances as function of SNR are shown in figure 10. It is evident that the detectability is extremely dependent on the relative PSD shapes of background and the noise to be detected, a fact that was noted and demonstrated also in [15]. Also, the background noise adding procedure used above gradually masks non-stationary fluctuations and creates a more stationary background which is deteriorating HMM detector performance for the 8 bar injection signals. We still found that these signals were detected also for a background noise that was increased by an additional 9 dB stationary noise. Taking into account the SNR_Δ this would correspond to an additive SNR of about -10 dB.

4.4. Detector demonstration

The HMM10233 detector was first tested on the pure background noise signals from recording 1. The responses (log conditional probabilities) on all sensors are shown in figure 11. To set a detection threshold, the following procedure was applied: As the output represents probabilities, it was fitted to a beta distribution. To be able to do so for these extremely small values, expressed on logarithmic scale, the following scaling relation was used, denoting the HMM log conditional probability output by $d_{HMM}(m)$

$$D(m) = K * e^{d_{HMM}(m)} \tag{13}$$

where K was a large constant. Then, the scaled output $D(m)$ was fitted to a beta distribution and a threshold corresponding to a false alarm rate of 10^{-8} was found by inspection of the cumulative distribution function. The obtained threshold was then inverse scaled back to the output region of $d_{HMM}(m)$. The same was done on all five sensor channels. The typical output level of $d_{HMM}(m)$ was around -150 for all channels when applied to a raw signal with Nyquist frequency of 12.8 kHz. The constant K was set to 10^{54} and the resulting thresholds ranged from -307 to -316, indicating robustness of the approach.

Due to impulsive events in the background noise, in total 5 false alarms on the $5 * 500 = 2500$ discriminant samples outside the training region were observed, corresponding to a false alarm rate of about 0.002. As none of these false alarms lasted longer than 1 second; it would probably be possible to decrease the false alarm rate on the Phenix steam generator background noise to a value much closer to the value of 10^{-8} obtained from the -316 threshold on the beta distribution fit.

The HMM10233 was then applied to the signal from sensor 1 for frequencies up to 12.8 kHz, using a threshold of -316, as found to be the minimum in the background noise study. The resulting discriminant is shown in figure 12. Noise changes which were judged to be due to argon bubbles circulating in the secondary circuit are detected abundantly after the first injection.

The HMM10233 was finally applied to the full injection test recordings (2-6) for all sensors and using full frequency data up to a Nyquist frequency of 25.6 kHz, resulting in the responses shown in figure 13.

5. Discussion

It is of importance to note that neither the ratio of driving argon pressure to the ambient pressure in the sodium line, nor the injector size were in these tests representative for a small leak. It has been demonstrated that apart from a low frequency whistle, the proposed acoustic anomaly detector here basically works as a bubble detector. A realistic small leak (around 1 g/s) would occur through a smaller orifice and with a higher pressure ratio since the secondary side of a steam generator is pressurized at 34-165 bar [1]. The aeroacoustic noise from such a leak will therefore be higher, both in terms of frequency and power, than the injections performed here [16], while the volume of bubbles produced

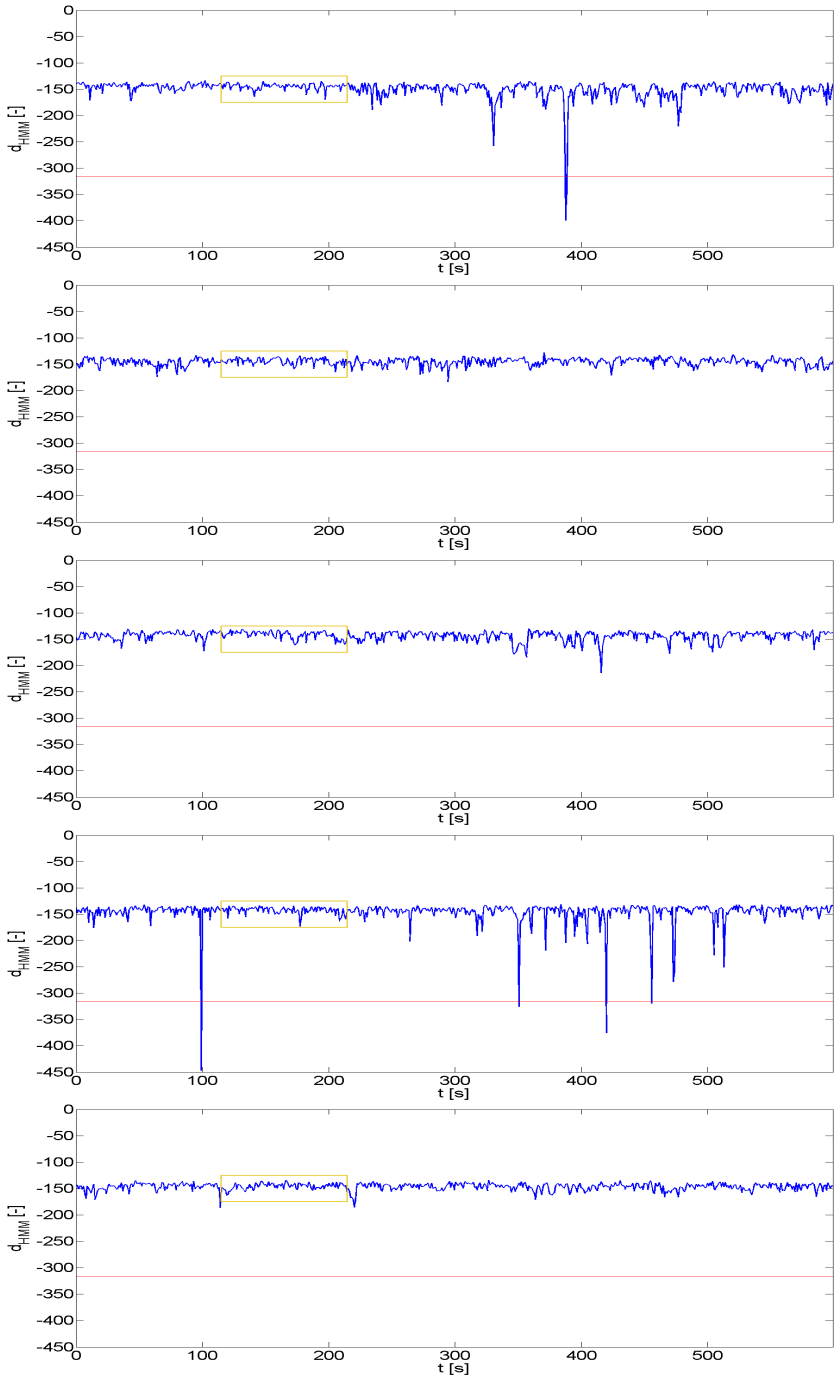


Figure 11: HMM discriminants on recording 1 (having a Nyquist frequency of 12.8 kHz). The HMM training region is indicated by a rectangle. The threshold was set by fitting a scaled version of d_{HMM} outside the training region to a beta distribution and requiring a theoretical false alarm rate of 10^{-8}

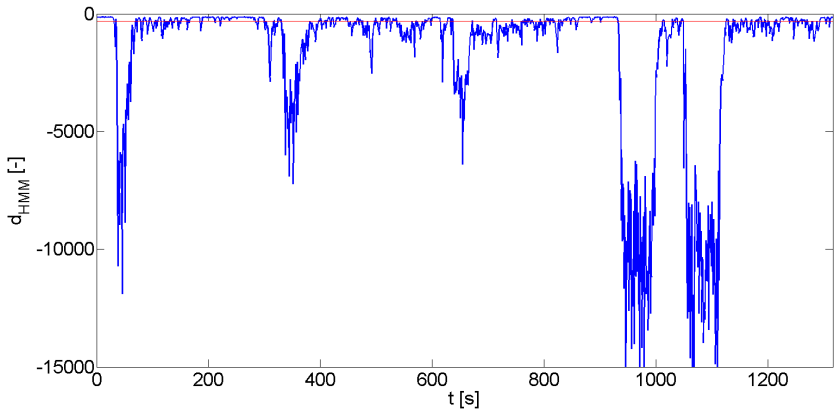


Figure 12: HMM discriminant on recordings 2-6 for sensor 1, using a downsampled raw signal with Nyquist frequency 12.8 kHz in order to be comparable to the background noise study.

will be smaller. Since the high detectability in terms of SNR of the gaussian white noise signal studied here is thanks to significant content in the higher frequency region where plant noise is relatively low, one could assume that real leaks would be detected with performance closer to this testing signal.

For the sodium-nitrogen heat exchanger developed by the CEA, the allowed detection delay can be extended to around one minute [5], thus making it likely that the proposed method will be sufficient for this application. In this case, using argon as a proxy for real nitrogen leaks is probably justifiable as both gases do not react chemically with sodium. For any unbuilt reactor system however, methods for reliable estimation of the acoustic SNR conditions of a small leak are however lacking. Also, if the detection system is required to function during operating point changes and transients, further development is also necessary. As the HMM concept is originally developed for classification of several different noise sequences (such as different words in speech recognition), it should be well suited also for this task but the resulting anomaly detection performance is not evident.

The procedure of parametrizing the detector used here (one parameter at a time) is rudimentary. The aim is to show that it can be done, using only background noise and relatively basic testing signals, and still arrive at a detector that performs well on real injection data. As stated in section 4.2 the procedure could be improved by using more testing signals and a responce surface method to find an optimal model. The parameter study is however time-consuming (on the order of several hours on the laptop computer used in this work) but in a real plant, it is reasonable to assume it needs to be performed only at first start-up. Re-training of the detector might have to be performed more often but should only take one or two minutes based on the computation times observed here.

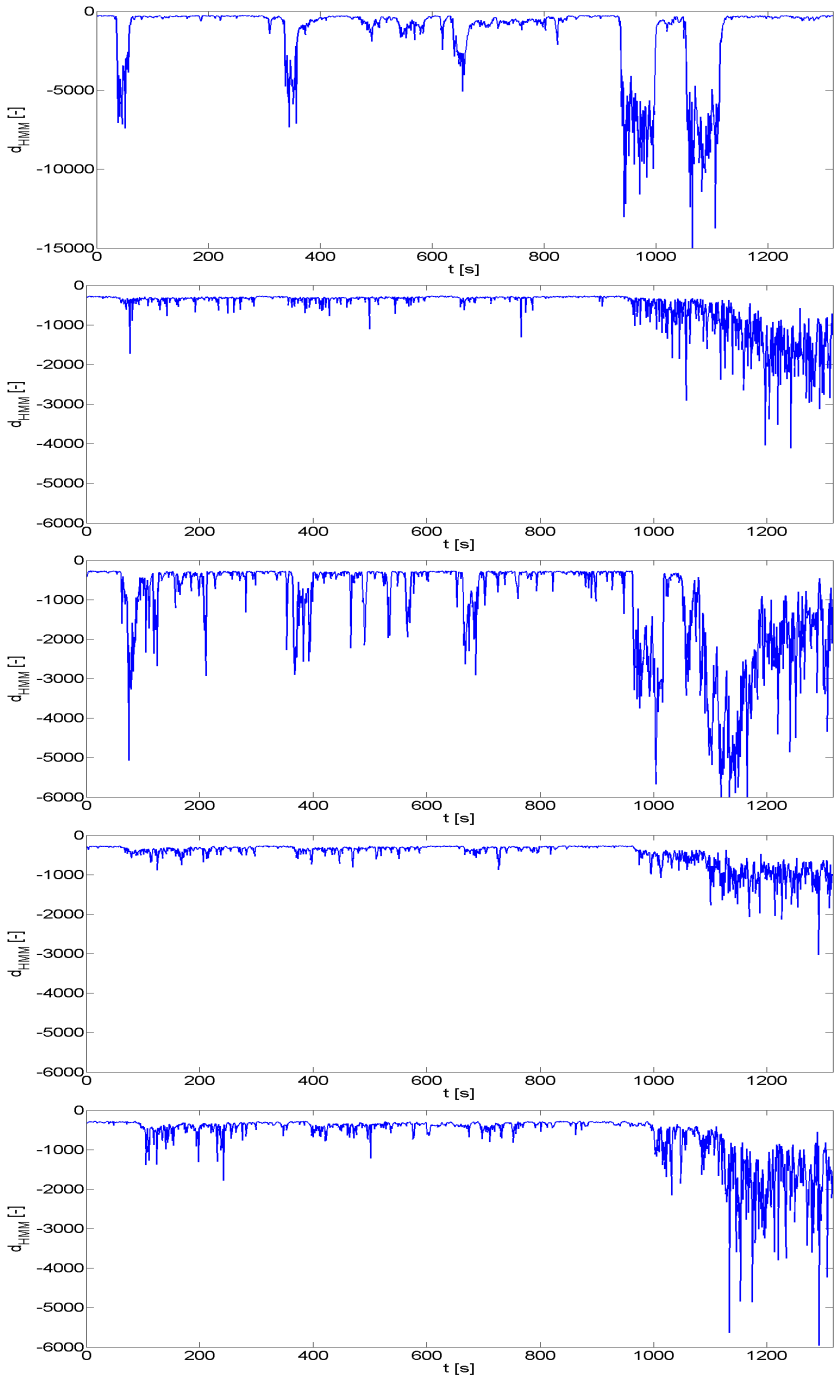


Figure 13: HMM discriminants on recordings 2-6 using the full raw signals with Nyquist frequency of 25.6 kHz.

6. Conclusions

A hidden Markov model method proposed earlier for passive acoustic leak detection in sodium fast reactor systems has been improved to eliminate ad-hoc setting of parameters and allow smaller amounts of training data. The improved method is verified to work well in a full power noise environment recorded during argon injection tests in the Phenix plant. The method is based on training a model on known background noise, i.e. without any assumptions on possible leak noise, and the free parameters of the model are set by a parametric study of detection performance for synthetic noises superposed on pure background noise.

The false alarm rate is governed not only by the detection method used, but also by the noise of the plant. For the 5x10 minutes of pure background noise studied here, the only sources of false alarms were impulsive events lasting about one second. By assuming an allowed detection delay of e.g. 3 seconds, it was thereby estimated that a false alarm rate close to the theoretical value of 10^{-8}, can be achieved on a single sensor channel. Regarding the minimum signal to noise ratio for detection, it has been shown that the 8 bar injection signals can be detected at conditions corresponding to an additive SNR of at least -10 dB. These results seem reasonable compared to the conclusions of [13], and [8] which were not based on realistic background noise and where the former work suffered from a lack of data preventing a credible false alarm rate estimation.

Possible ways of improving passive acoustic detector performance further would be to specifically monitor high-frequency regions where background noise can be expected to be relatively low (if leak noise can be expected in this region). Multi-sensor methods using adaptive filtering and/or spatial focalisation techniques such as beamforming also represent possibilities for further improvement.

In order to increase the maturity of this research field further, it is also of interest to study methods for estimating SNR conditions of leaks in a given system and to develop detection methods that will work also during operating point changes. Finally, even if the method proposed here is independent on knowledge on possible leak noise, such knowledge will remain of large interest to motivate monitoring of particular frequency regions and thereby increase performance further if needed.

7. Acknowledgments

This study was performed within the framework of an ongoing collaboration project between KTH and CEA on the instrumentation and safety of sodium cooled reactors, supported by the Swedish Research Council, grant number B0774801.

8. References

[1] International Atomic Energy Agency, *Liquid metal reactors: Experience in design and operation*, IAEA-TECDOC-1569, International Atomic Energy Agency, 2007

[2] International Atomic Energy Agency, *Acoustic signal processing for the detection of sodium boiling or sodium-water reaction in LMFRs*, IAEA-TECDOC-946, International Atomic Energy Agency, 1997

[3] J.P. Jeannot, T. Gnanasekaran, C. Latge, R. Sridharan, L. Martin, R. Ganesan, J.M. Augem, JL. Courouau and G. Gobillot, *In-sodium hydrogen detection in the Phenix fast reactor steam generator: A comparison between two detection methods*, ANIMMA International Conference, Marseille, France, 7-10 June 2009

[4] N. Matta, Y. Vandenboomgaerde and J. Arlat, *Supervision and Safety of Complex Systems*, ISTE Ltd and John Wiley & sons Inc., ISBN: 978-1-84821-413-2 , 2012

[5] J.L. Perrin, *Projet ASTRID. Cahier des Charges Fonctionnel du Réacteur ASTRID*, CEA/DEN/CAD/DER/CPA AST2 AST NT CPA 024 - Indice 4, 2014

[6] V.S. Yughay, R.F. Masagutov and F.A. Kozlov, *Acoustic effects from water leaking into sodium*, Atomnaya Energiya, Vol. 54, No. 3, pp. 170-173, 1983

[7] S. Hur, D.H. Kim, S.H. Seong and S.O. Kim, *Measurement strategy of the water leakage into a low pressure sodium boundary for a liquid metal reactor*, Key Engineering Materials, Vol. 270-273, pp. 518-524, 2004

[8] A.R. Marklund, S. Kishore, V. Prakash, K.K. Rajan and F. Michel, *Passive Acoustic Leak Detection for Sodium Cooled Fast Reactors Using Hidden Markov Models*, IEEE Transactions on Nuclear Science, Published online February 19th, 2016

[9] O. Descombin, *Détection acoustique d'une réaction sodium eau (RSE) dans les générateurs de vapeur (GV) des RNR : Etat de l'art en 2010*, CEA/DEN/CAD/DTN/STPA/LIET/2011/007, 2011

[10] L. R. Rabiner, *A tutorial on hidden Markov models and selected applications in speech recognition*, Proceedings of the IEEE, Vol. 77, No. 2, pp. 257-285, 1989

[11] A. Leijon, *Pattern recognition - fundamental theory and exercise problems*, KTH Electrical Engineering, 2010

[12] P.D. Welch, *The Use of Fast Fourier Transform for the Estimation of Power Spectra: A Method Based on Time Averaging Over Short Modified Periodograms* IEEE Trans. Audio Electroacoustics, Vol. AU-15, pp.70-73, 1967

[13] A.R. Marklund and F. Michel, *Application of a new passive acoustic leak detection approach to recordings from the Dounreay prototype fast reactor*, Annals of Nuclear Energy, Vol. 85, pp. 175-182, 2015

[14] T. Fawcett, *An introduction to ROC analysis*, Pattern Recognition Letters, Vol. 27, pp. 861874, 2006

[15] A.R. Marklund and J. Dufek, *Development and comparison of spectral methods for passive acoustic anomaly detection in nuclear power plants*, Applied acoustics, Vol. 83, pp. 100-107, 2014

[16] K.B.M.Q. Zaman and J.C. Yu, *Power spectral density of subsonic jet noise*, Journal of Sound and Vibration Vol. 98, No. 4, pp. 519-537, 1985